

Generating Humanoid Multi-Contact through Feasibility Visualization

Stephen McCrory^{1,2}, Sylvain Bertrand¹, Achintya Mohan³, Duncan Calvert^{1,2}, Jerry Pratt⁴, Robert Griffin^{1,2}

Abstract—We present a feasibility-driven teleoperation framework designed to generate humanoid multi-contact maneuvers for use in unstructured environments. Our framework is designed for motions with arbitrary contact modes and postures. The operator configures a pre-execution preview robot through contact points and kinematic tasks. A fast estimation of the preview robot’s quasi-static feasibility is performed by checking contact stability and collisions along an interpolated trajectory. A visualization of Center of Mass (CoM) stability margin, based on friction and actuation constraints, is displayed and can be previewed if the operator chooses to add or remove contacts. Contact points can be placed anywhere on a mesh approximation of the robot surface, enabling motions with knee or forearm contacts. We demonstrate our approach in simulation and hardware on a NASA Valkyrie humanoid, focusing on multi-contact trajectories which are challenging to generate autonomously or through alternative teleoperation approaches.

I. INTRODUCTION

Humanoid robots are frequently designed to be capable of a wide range of motions. Making full use of these platforms as well as understanding their limitations requires an ability to generate and deploy coordinated, multi-contact maneuvers. Generating such motions is achieved by relaxing assumptions about the robot’s posture, contactable limbs and contact modes (e.g. planar, line or point contacts) in order to maintain motion generality. The quasi-static case has been well-studied and mature tools exist for reasoning about arbitrary friction constraints [1], admissible trajectory timing [2], and actuation margins [3]. However, leveraging these tools for search-based planning presents a number of obstacles. Primarily, multi-contact motions have an inherently large branching factor which can cause planning to be computationally intractable or rely on heuristics [4, 5]. Additionally, it is challenging to construct generic posture scoring functions that perform well over a large space of configurations. In this work we present a teleoperation framework which builds on existing multi-contact feasibility metrics, namely [1, 3], by providing feasibility visualization to the operator. The operator guides the trajectory using contact and posture tasks and is informed of motion feasibility during teleoperation.

This work was supported through ONR Grant No. N00014-19-1-2023 and NASA Grant No. 80NSSC20M0197.

¹ Author is with the Institute of Human and Machine Cognition (IHMC), 40 S Alcaniz St, Pensacola, FL 32502, USA

² Author is with the University of West Florida (UWF), 11000 University Pkwy, Pensacola, FL 32514, USA

³ Author is with Georgia Institute of Technology, North Avenue Atlanta, GA 30332, USA

⁴ Author is with Figure AI, Inc., Sunnyvale, CA

Email: {smccrory, sbertrand, dcalvert, jpratt, rgriffin}@ihmc.org, achintya@gatech.edu

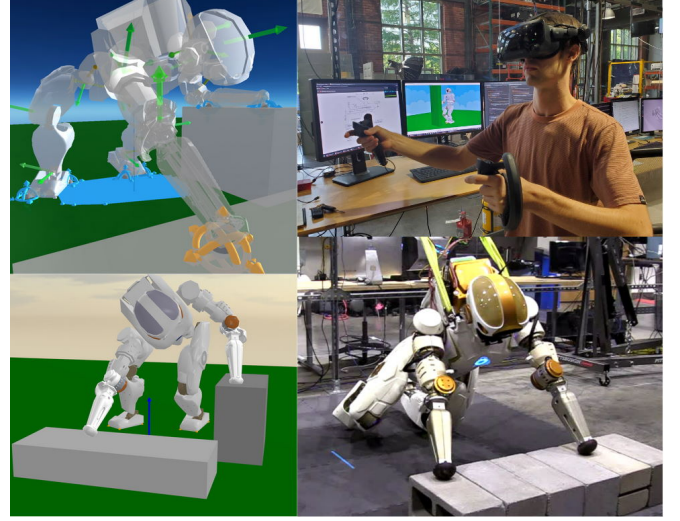


Fig. 1: Demonstration of the presented teleoperation framework on Valkyrie in various multi-contact scenarios. The operator (top-right) uses a VR application (top-left) to iteratively create keyframes by dragging a preview robot to the desired configuration. Trajectories are validated in simulation (bottom-left) and hardware (bottom-right) on the Valkyrie humanoid.

The aim of this teleoperation approach is to capture a wide family of multi-contact maneuvers, including crawling, kneeling, bracing against a wall as well as normal standing. In addition to the contact and actuation feasibility checks mentioned above, these motions require a flexible interface for generating atypical contacts and postures. In our interface, the operator can generate contact points anywhere on the surface of a mesh approximation of the robot. Similarly, taskspace posture setpoints can be generated for any link, with configurable priority weighting and constrained axes.

The presented work is implemented as a Virtual Reality (VR) interface. Our design prioritizes flexible operator input and visualizing spatial artifacts, matching many strengths of VR. Research has shown VR offers flexible and expressive operator input when manipulating virtual artifacts [6] and has been shown to reduce operation time compared to conventional desktop interfaces [7]. However, our approach is not unique to VR and the presented results are independent of the use of VR. We validate our interface in three simulated teleoperation experiments in which the robot performs multi-contact maneuvers. For experiment two, we deploy the motion on a physical Valkyrie robot to perform a crouch-to-kneel motion.

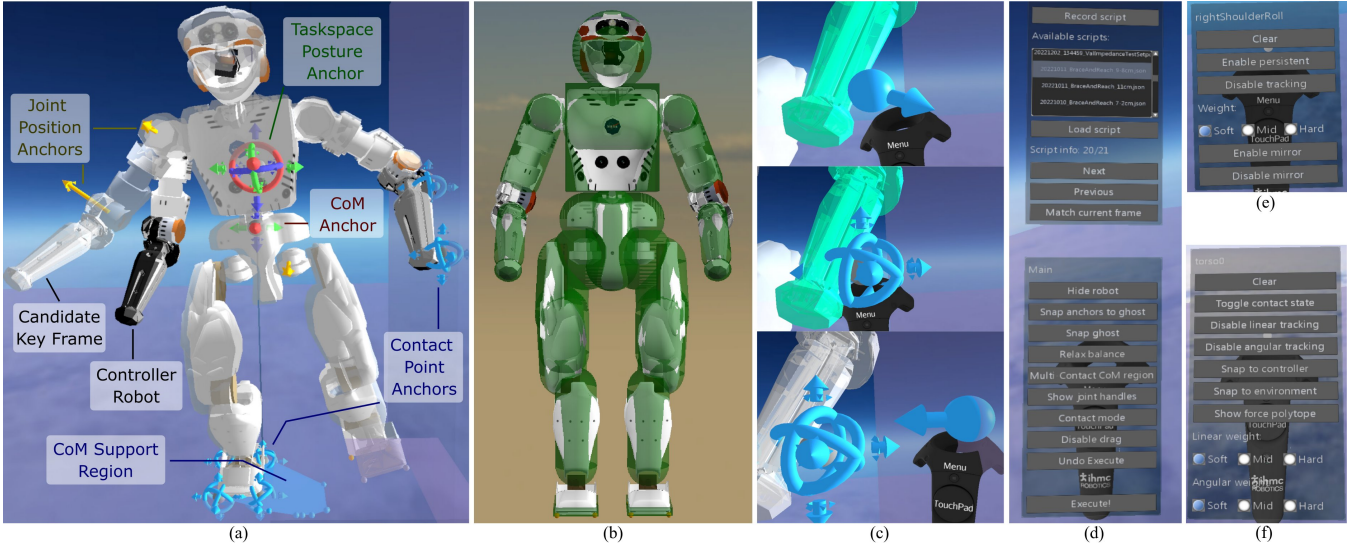


Fig. 3: (a) Operator view in VR with Valkyrie leaning against a wall. (b) Convex mesh model of Valkyrie. Taskspace posture anchors are generated with a control frame that lies inside the shape(s) corresponding to the configured link. Similarly, contact point anchors are generated along the surface of the shape(s) corresponding to the contacting link. (c) Contact points are projected to the surface of the robot or environment mesh while creating (top) or placing (bottom) a contact point anchor. The arrow indicates the surface normal of the robot or environment mesh. (d) Main menu used to export/load keyframe scripts, toggle visualization, configure solver behavior and switch between placing taskspace posture and contact anchors. (e) Joint anchor menu. (f) Taskspace posture/contact point anchor menu.

Keyframes are generated in VR by configuring a set of kinematic tasks, such as desired contact state, taskspace posture, preferred joint angles and CoM position. An inverse kinematics (IK) solver continuously processes these inputs and computes the candidate keyframe along with an interpolated trajectory. The operator receives real-time feedback based on 3 feasibility metrics: (1) the set of contacts that are currently removable, (2) the static stability and collision status of the keyframe and (3) the static stability and collision status of the interpolated trajectory to the keyframe. The feasibility estimation is then displayed to the user along with relevant data such as CoM stability margin and joint actuation saturation. When a user is finished configuring the candidate keyframe and the feasibility estimation is valid, it can be dispatched to the robot.

A. Kinematic Task Generation

The VR interface is designed to enable an operator to pose the robot by creating, removing or modifying constraints on-the-fly. To do this, four types of virtual interactable “anchors” are available, each corresponding to a type of kinematic task (Fig 3(a)):

- **Taskspace Posture:** Matches a reference frame F_p that is rigidly attached to link l with a desired frame F_d expressed in world coordinates.
- **Center of Mass:** Matches the robot’s CoM with a desired position expressed in world coordinates.
- **Joint Position:** Matches to a preferred joint angle.
- **Contact Point:** Matches a contact point p_c that is rigidly attached to link l with a desired position p_d in world coordinates.

An approximate convex decomposition of the robot’s mesh (Fig. 3(b)) is used to aid the link-VR controller association.

When the VR controller enters a convex shape of the preview robot, the corresponding link l is highlighted and the user can click to generate a taskspace control frame F_p at the VR controller’s pose, which is initially coincident with F_d . The virtual anchor, which represents F_d , can then be dragged and rotated to the desired pose. The user can toggle which of the three linear and angular constraint axes are enabled, reflected visually with highlights on the anchor (Fig. 3(a)).

The CoM anchor is created by selecting a marker designating the candidate keyframe’s current CoM. Similar to the taskspace posture anchor, the user can enable which linear axes are constrained. Joint position anchors can be enabled for any joint and are primarily used to bias the IK solver within a nullspace. All kinematic tasks are assigned a relative priority level by specifying one of soft, mid or hard weights, which are set through anchor menus (Fig. 3(e,f)). The option to “Snap anchors to ghost” (Fig. 3(d)) will move the setpoint of all non-contact kinematic tasks to the currently achieved IK configuration.

B. Contact Points

Contact point anchors are created in a specific mode which projects the VR controller positions to the surface of the nearest convex shape of the preview robot (Fig. 3(b)), with an arrow showing the surface normal. Environment shapes are also modelled as convex shapes. Contact points can be snapped to the environment using a similar mode that projects the VR controller to the surface of the nearest environment shape and shows the environment surface normal. Fig. 3(c)-top shows a contact point being created on the robot’s forearm and Fig. 3(c)-bottom shows the contact point being snapped to a wall. Line and plane contacts are created by configuring the set of contact points accordingly.

IV. KINEMATICS SOLVER

An optimization-based IK solver is used to compute quasi-statically stable whole-body configurations given a set of kinematic tasks. We solve the IK problem using Sequential Quadratic Programming (SQP) due to its generality and success on humanoids [8, 9, 23]. At every solve step, a desired velocity $\mathbf{v}_d \in \mathbb{R}^{n+6}$ is computed to drive the model towards a configuration that achieves the desired task objectives, where n is the number of actuated degrees of freedom in the robot. Note that \mathbf{v}_d represents the velocity of the solver model and is independent of the controller's velocity. The IK iteratively solves the following Quadratic Program (QP):

$$\begin{aligned} \min_{\mathbf{v}_d} \quad & c_{\text{nom}} + \mathbf{c}_J + \mathbf{c}_{\mathbf{v}_d} \\ \text{s.t.} \quad & \mathbf{v}_{\min} \leq \mathbf{v}_d \leq \mathbf{v}_{\max} \end{aligned} \quad (1)$$

The objective function terms are given by:

Nominal Objective: $c_{\text{nom}} = (\mathbf{v}_d - \mathbf{v}_{\text{nom}})^T \mathbf{C}_{\text{nom}} (\mathbf{v}_d - \mathbf{v}_{\text{nom}})$

Kinematic Tasks: $\mathbf{c}_J = (\mathbf{J}\mathbf{v}_d - \mathbf{p})^T \mathbf{C}_J (\mathbf{J}\mathbf{v}_d - \mathbf{p})$

Velocity Cost: $\mathbf{c}_{\mathbf{v}_d} = \mathbf{v}_d^T \mathbf{C}_{\mathbf{v}_d} \mathbf{v}_d$,

where the terms are given by:

- \mathbf{v}_{nom} drives the robot to a nominal whole-body configuration, which by default is the controller's current configuration. The user can set the nominal configuration as IK's current solution as by selecting "snap ghost" (Fig. 3(d)), which is generally used for larger motions where the controller and IK differ significantly.
- $\mathbf{J} = [\mathbf{J}_1^T \dots \mathbf{J}_k^T]^T$ and $\mathbf{p} = [\mathbf{p}_1^T \dots \mathbf{p}_k^T]^T$ are the stacked Jacobian matrices and motion objectives computed as feedback terms from the kinematic tasks and $\mathbf{C}_J = \text{diag}(\mathbf{w}_0, \dots, \mathbf{w}_k)$ is a block-diagonal weight matrix, which is detailed below.
- \mathbf{v}_{\min} and \mathbf{v}_{\max} bound the joint velocity so the joint remains within its bounds within the update period ΔT .
- $\mathbf{C}_{\text{nom}} = 0.5 \mathbf{I}_{n+6}$ and $\mathbf{C}_{\mathbf{v}_d} = 0.1 \mathbf{I}_{n+6}$ are constant weight matrices.

With each solve iteration, the candidate keyframe configuration \mathbf{q}_d is updated by integrating the computed velocities (Eq. 2), where ΔT is the solver update period.

$$\mathbf{q}_d \leftarrow \mathbf{q}_d + \mathbf{v}_d \Delta T \quad (2)$$

For kinematic task i , a task Jacobian \mathbf{J}_i and feedback motion \mathbf{p}_i are used to compute a feedback term:

- Joint Position: \mathbf{J}_i is a selection matrix for the joint and \mathbf{p}_i is a velocity proportional to the position error.
- Center of Mass: \mathbf{J}_i is the linear centroidal momentum matrix \mathbf{A} [24] and the objective \mathbf{p}_i is a momentum proportional to the linear position error.
- Taskspace Posture and Contact Point: \mathbf{J}_i is the geometric Jacobian [25] of the control frame F_p (Sec. III-A). A proportional feedback law on the relative transform between F_p and F_d is used to compute \mathbf{p}_i [26].

Kinematic tasks are each assigned a weight matrix $\mathbf{w}_i = w_i \mathbf{I}_{N_i}$, where w_i is computed from the task's priority given by Tab. II and N_i is the tasks's dimensionality. Note that

TABLE II: Kinematic Task Weights

	Soft	Mid	Hard
Taskspace Posture	0.1	1.0	10.0
CoM	0.01/ m	0.1/ m	1.0/ m
Joint Position	0.1	1.0	10.0
Contact Point	50.0	200.0	500.0

the CoM task weight is scaled down by the robot mass m so feedback is only dependent on kinematic quantities. For Taskspace Posture, Center of Mass and Contact Points, a selection matrix \mathbf{S}_i is used to only provide feedback for the constrained axes. This is done by premultiplying both the Jacobian and objective by \mathbf{S}_i .

V. FEASIBILITY ESTIMATION

During teleoperation, motion feasibility is assessed for the candidate keyframe and keyframe transition. In V-A we present our approach for assessing the CoM stability margin [1, 3] based on the preview robot's state. In V-B we present our method for anchor-based kinematic interpolation. In V-C we then present our approach for visual feasibility cues which are based on three motion feasibility checks: contact removal feasibility, keyframe configuration feasibility and keyframe transition feasibility.

A. CoM Stability Margin

The set of contact point anchors describes the candidate keyframe's contact state. A contact anchor i is parameterized by a contact point position \mathbf{r}_i , contact normal \mathbf{n}_i and contact force \mathbf{f}_i . The jointspace rigid body equations of motion [27] for the quasi-static case of $\ddot{\mathbf{q}} \approx \dot{\mathbf{q}} \approx \mathbf{0}$ are given by:

$$\mathbf{G} - \boldsymbol{\tau} = \sum_{i=1}^{N_c} \mathbf{J}_{c,i}^T \mathbf{f}_i = \mathbf{J}_c^T \mathbf{f}. \quad (3)$$

Where N_c is the number of contact points, \mathbf{G} is the gravitational torque vector, $\boldsymbol{\tau}$ are the set of joint torques, and $\mathbf{J}_{c,i} \in \mathbb{R}^{3 \times n}$ is the Jacobian for contact i . A stacked contact Jacobian \mathbf{J}_c and force vector \mathbf{f} are used for brevity. For a given keyframe, static equilibrium is expressed as the feasibility problem:

$$\begin{aligned} \exists \mathbf{f} \text{ s.t.} \quad & \mathbf{f}_i \in \mathcal{K}_i \\ & \sum_i \mathbf{f}_i = -m\mathbf{g} \\ & \sum_i \mathbf{r}_i \times \mathbf{f}_i = -\mathbf{c} \times (m\mathbf{g}) \\ & \mathbf{G} - \boldsymbol{\tau}^+ \leq \mathbf{J}_c^T \mathbf{f} \leq \mathbf{G} - \boldsymbol{\tau}^-, \end{aligned} \quad (4)$$

where \mathcal{K}_i is the friction cone of contact i , $\mathbf{g} = (0, 0, -9.81)^T$ is gravitational acceleration, \mathbf{c} is the CoM position and $\boldsymbol{\tau}^-, \boldsymbol{\tau}^+$ are the lower and upper joint torque bounds. The standard linearized friction model [5] is used so that Eq. 4 contains only linear constraints. Using this set of linear constraints, we compute the preview robot's CoM stability margin using the Iterative Projection algorithm introduced by Bretl et al. [1]. This approach recursively solves a Linear Program to compute maximal CoM displacements along a

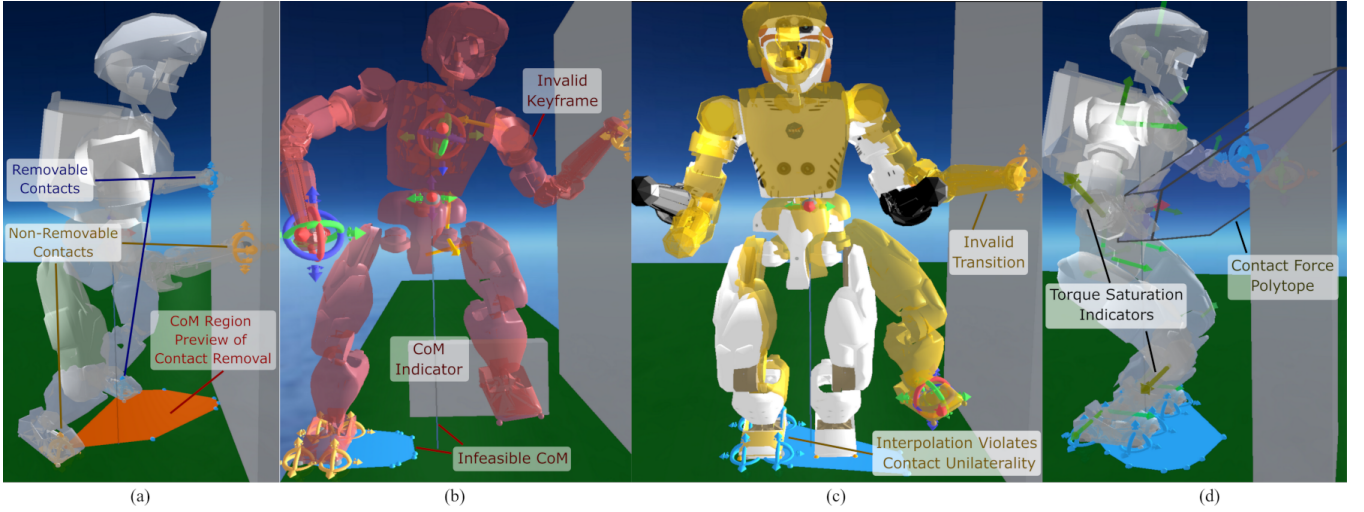


Fig. 4: (a) Contact anchor color indicates whether a contact is removable. The operator can select a contact and preview the CoM region in the absence of the contact. The CoM region shown is a preview with the right arm contact removed, which is currently infeasible. The preview robot turns red if a keyframe is invalid (b) or yellow if the keyframe transition is invalid. In (c), although the keyframe is valid, the keyframe transition requires the CoM to leave the CoM feasible region before placing the left hand. (d) Actuation feasibility can be visualized by a force polytope at contact points and by indicating joint torque saturation. In this figure the right knee and elbow are a darker shade, indicating they are close to torque saturation.

set of query directions (see Appendix for details on region calculation). If the preview robot’s CoM is inside this region, it indicates the posture is quasi-statically stable with respect to friction and actuation constraints.

B. Kinematic Interpolation

Kinematic interpolation is done by computing a set of intermediate whole-body configurations that smoothly blend the kinematic task sets between two consecutive keyframes K_0 (start) and K_1 (end). To do this, each kinematic task is assigned a corresponding task on the opposite side of interpolation. While this is trivial for tasks expressed in both K_0 and K_1 , we create additional “placeholder” tasks for those only present in K_0 or K_1 . The placeholder task corresponding to task T is given zero weight and a setpoint equal to T expressed in the opposite keyframe. For example, if a taskspace posture task for the hand is present in K_0 but not K_1 , the placeholder setpoint is the frame F_p on the hand expressed in K_1 .

The intermediate configurations are computed by interpolating along discrete, evenly-spaced points parameterized by a phase variable $s = \frac{i}{N_I+1}, i = \{1, 2, \dots, N_I\}$. Kinematic task weights are interpolated using the formula:

$$w(s) = w_0(1-s)^{\alpha_0} + w_1s^{\alpha_1}, \quad (5)$$

where w_0 and w_1 are the kinematic task’s weight at the start and end of interpolation and α_0, α_1 are tuning parameters. Kinematic task setpoints are interpolated linearly for spatial and joint positions. Orientation setpoints are interpolated using Spherical Linear Interpolation (Slerp) [28]. Additionally, for joints that do not contain a nominal task we create a joint position task to bias the start and end of interpolation to match the keyframe configurations with a fixed bias weight

of $w_b = 1.5$ and tuning exponent $\alpha = 6$. In all other cases, weights are interpolated linearly with $\alpha = 1$.

We find that a value $N_I = 12$ is sufficient for validating transitions between consecutive keyframes due to sufficient resolution while still yielding a fast computation time of 77ms (see Tab. III). For $N_I = 12$, we observe an average deviation of 2mm for contacting links and 4mm for non-contacting links when compared to interpolating at significantly higher values of N_I .

Contact switches occur at either the start or end of interpolation. Therefore, the active set of contact points during interpolation are contact points present in both K_0 and K_1 .

C. Feasibility Visualization

To compute if a contact is removable, a modified feasible CoM region is computed with the given contact removed. A contact is considered removable only if the CoM is contained in the modified feasible region. Removability is continuously updated for all contacts as the keyframe configuration changes and non-removable contacts are marked visually and cannot be removed. The operator can select a contact and preview the CoM feasible region if it were removed in order to adjust the CoM accordingly before removing a contact as shown in Fig. 4(a).

The candidate keyframe and the N_I interpolated configurations are checked for kinematic and static feasibility. Each of the $(1 + N_I)$ configurations has the following checks:

- Kinematics-Statics solver (Eq. 1) cost converges such that successive costs are within a bound $\epsilon_{ik} = 10^{-5}$.
- Contact point anchors track with a bound $\epsilon_c = 10^{-3}$ m.
- The feasible CoM region contains the CoM, indicating friction and actuation constraints are statically achieved.
- Configuration has no environment collisions among non-contacting links.

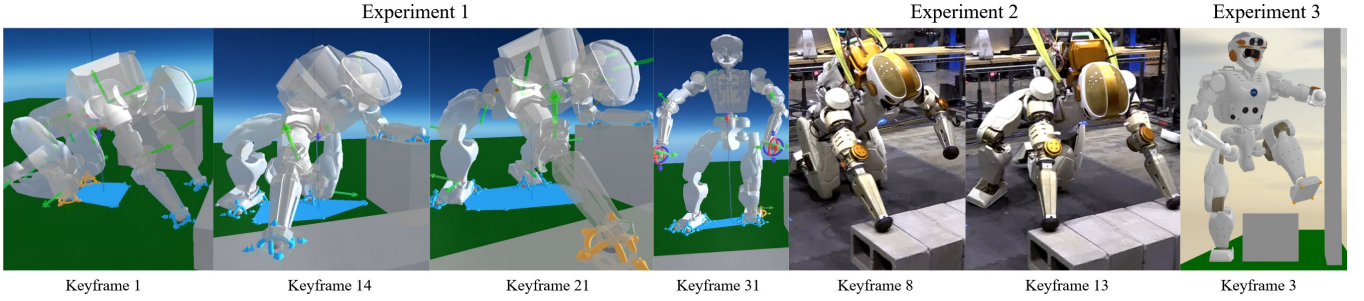


Fig. 5: Experiment 1 (simulation): the robot was teleoperated from an initial crouching stance to standing with handholds available in front and to the left of the robot. Experiment 2 (hardware): a modification of the experiment 1 script was deployed to a physical Valkyrie robot. The robot places both hands on the cinder blocks and lifts the right knee to place the right foot on the ground. Experiment 3 (simulation): the robot braces against a wall using the forearm and swings the left foot over an obstacle.

The preview robot color is modified to reflect whether the candidate keyframe or transition is infeasible. In the event the preview robot is near actuation limits, the operator is also aided by visual cues to determine the joint that is actuation-limited and how to adjust the posture (Fig. 4(d)). Given the candidate keyframe’s contact state, a static force distribution \mathbf{f}_g is computed (see Appendix for details). The corresponding joint torques $\boldsymbol{\tau}_g$ are computed from Eq. 3:

$$\boldsymbol{\tau}_g = \mathbf{G} - \mathbf{J}_c^T \mathbf{f}_g. \quad (6)$$

The color of joint position anchors is updated so that elements of $\boldsymbol{\tau}_g$ near the torque bounds are colored red to alert the operator. The force polytope \mathcal{P}_i at a contact anchor i can also be visualized, given by [29]:

$$\mathcal{P}_i = \{\mathbf{f}_i \in \mathbb{R}^3 \mid \boldsymbol{\tau}^- \leq \mathbf{J}_{c,i}^T \mathbf{f}_i \leq \boldsymbol{\tau}^+\}. \quad (7)$$

This can be useful if the polytope’s “major axis” has an intuitive preferred orientation, such as vertical when contacting the ground or horizontal when bracing against a wall.

VI. RESULTS

A. Framework Timing

The teleoperation framework divides computation among three threads: a kinematics-statics thread that computes Eq. 1, a VR thread and a transition feasibility thread. The VR application is run on a Valve Index [30] at a refresh rate of 90Hz. We use Java Monkey Engine [31] for scene graphics. The execution times of various tasks in the framework were measured and are reported in Tab. III. Each reported time is the average over a window of 100 updates. The evaluation was performed on a desktop with a 10th gen 10-core i9 processor (3.70 GHz). This was measured under a nominal operating condition while standing with 8 contact anchors, two taskspace posture anchors, two joint position anchors and a CoM anchor.

B. Experiment 1: Crouch to Stand, Simulated

We tested² our teleoperation framework in a simulated scenario where Valkyrie starts in a crouched position on the

²A video of the teleoperation is available at <https://www.youtube.com/watch?v=AJ1SsU4TvkK>

TABLE III: Timing Evaluation

Task	Description	Time (ms)
Kinematics-Statics Solver	Total	4.63
	CoM Region	4.05
	Kinematics Solver	0.58
VR Interface	Total	5.81
	VR API	2.00
	Kinematic Task Processing	1.06
	Collision Check	0.06
	Contact Removal	2.43
	Gravity Compensation Torques	0.26
Transition Feasibility	Total	77.3

ground next to two flat boxes, to the front and left of the robot. Tab. IV shows the teleoperation statistics, including anchor count and achieved contact modes. As shown on the bottom rows, significant use of line contacts was made in addition to point and plane contacts. Fig. 5 highlights important keyframes and contact modes. In keyframe 14, the left forearm is supported through a line contact between the elbow and hand. Also in keyframe 14, the right foot forms a line contact on the inside edge of the foot. In keyframe 21, the front edge of the left foot forms a line contact while placing the foot down. The trajectory was executed using a whole-body impedance controller at 2s per keyframe with an average joint tracking (0.0043 ± 0.002)rad.

C. Experiment 2: Crouch to Kneel, Simulated with Hardware Validation

We deployed a modified version of the keyframe sequence in Experiment 1 to a physical Valkyrie robot. The sequence starts in the same configuration but only has a front block, as forearm contact on the left block was not possible due to exposed wiring. The same three initial events are present as in Experiment 1: place right hand, place left hand and place right foot. As shown in Fig. 5, triple support between two knees and a single hand contact were achieved while placing a hand on the blocks (keyframe 8). Additionally, line contact on the right foot was made while placing the foot down (keyframe 19). The trajectory is tracked at 4s per keyframe using an impedance controller which modulates gains based on limb loading (see Appendix) and achieved an average joint tracking of (0.023 ± 0.009)rad. This experiment was

TABLE IV: Experiment 1 Statistics Simulated Crouch to Stand. Operation Time: 16m18s.

	Keyframe	1	2	3	4	5	6	7	8	9	10	11	12	13	14	15	16	17	18	19	20	21	22	23	24	25	26	27	28	29	30	31
TaskSpace	Event	Place R. Hand				Place L. Hand/Elbow				Place R. Foot				Lift L. Knee, Place L. Foot						Lift L. Elbow			Lift R. Hand			Lift L. Hand						
	Total	0	1	1	0	0	1	1	1	0	0	1	0	0	0	1	1	0	0	0	0	0	1	1	0	0	0	1	1	1	2	2
	Modified	-	-	1	-	-	-	1	1	-	-	-	-	-	-	-	1	-	-	-	-	-	-	-	-	-	-	-	-	-	-	-
	Add/Rem.	-	+1	-	-1	-	+1	-	-	-1	-	+1	-1	-	-	+1	-	-1	-	-	-	-	+1	-	-1	-	-	-	+1	-	-	-
Joint	Total	4	5	5	5	5	6	5	5	6	6	9	10	4	4	4	7	6	6	7	2	2	2	3	3	3	3	3	4	4	4	4
	Modified	-	-	1	-	-	-	-	-	-	1	-	1	3	-	-	-	1	2	3	4	1	-	-	-	-	-	-	1	-	-	-
	Add/Rem.	-	+1	-	-	-	+1	-1	-	+1	-	-	+3	+1	-6	-	-	+3	-1	-	+1	-5	-	-	+1	-	-	+1	-	-	-	-
CoM	Enabled	✓	✓	✓	✓	✓	✓	✓	✓	✓	✓	✓	✓	✓	✓	✓	✓	✓	✓	✓	✓	✓	✓	✓	✓	✓	✓	✓	✓	✓	✓	✓
	Modified	✓	✓	✓	✓	✓	✓	✓	✓	✓	✓	✓	✓	✓	✓	✓	✓	✓	✓	✓	✓	✓	✓	✓	✓	✓	✓	✓	✓	✓	✓	✓
Contact	Total	4	3	3	4	4	3	3	3	4	5	4	4	4	6	5	6	6	6	6	6	7	6	6	7	7	7	6	7	7	6	6
	Modified	-	-	-	-	-	-	-	-	-	1	-	-	-	2	-	-	-	-	-	-	-	-	-	-	-	-	-	-	-	-	-
C. Mode	Add/Rem.	-	-1	-	+1	-	-1	-	-	+1	-1	-	-	-	+2	-1	+1	-	-	-	-	+2,-1	-1	-	+1	-	-	-1	+1	-	-1	-
	Point	4	3	3	4	4	3	3	3	4	3	2	2	2	2	1	1	1	1	1	1	1	2	2	2	2	2	1	1	1	-	-
	Line	-	-	-	-	-	-	-	-	-	1	1	1	1	2	2	1	1	1	1	1	2	1	1	1	1	1	1	1	-	-	-
	Plane	-	-	-	-	-	-	-	-	-	-	-	-	-	-	-	1	1	1	1	1	1	1	1	1	1	1	2	2	2	2	2

performed by first teleoperating the robot in simulation, then deploying the trajectory to Valkyrie. Deploying to hardware serves as empirical verification of the presented feasibility checks as well as simulation accuracy. Using this framework for live hardware teleoperation will be pursued in future work and was not performed due to hardware safety concerns.

D. Experiment 3: Bracing Against a Wall, Simulated

For experiment 3, the robot stands on a narrow platform with a wall on the side and 34cm tall obstacle blocking the path. The robot braces against the wall with the left forearm while swinging the left foot over the obstacle (Fig. 5). The use of the left elbow contact reduces load on the elbow joint from 40-55Nm (without elbow contact) to 15-25Nm (with elbow contact). In this scenario, CoM feasibility plays a crucial role as the robot is swinging its foot (Fig. 6). During the motion, the feasible CoM region changes on an order of 10cm as the posture, namely the supporting limb Jacobians, are changing. This highlights a case where CoM feasibility is not intuitive and the operator relies on the automated feasibility checks during teleoperation. The trajectory was executed using a whole-body inverse dynamics controller at 2s per keyframe with an average joint tracking of (0.036 ± 0.008) rad.

VII. DISCUSSION AND FUTURE WORK

The presented framework demonstrates a teleoperation strategy designed around maximizing the set of user-commandable contact and kinematic constraints. We demonstrated the effectiveness of this strategy by teleoperating in scenarios that are difficult or impossible without the use of knee/elbow contacts, line contacts and arbitrary taskspace objectives. Through real-time feasibility assessment, the operator was able to successfully teleoperate in scenarios where human intuition is likely insufficient.

Future work will focus on further decreasing operator burden through a number of improvements. One is through explicit modeling of contact modes. In addition to decreasing contact creation time, this allows enumerating contact mode transitions, such as the plane-to-line transition when during

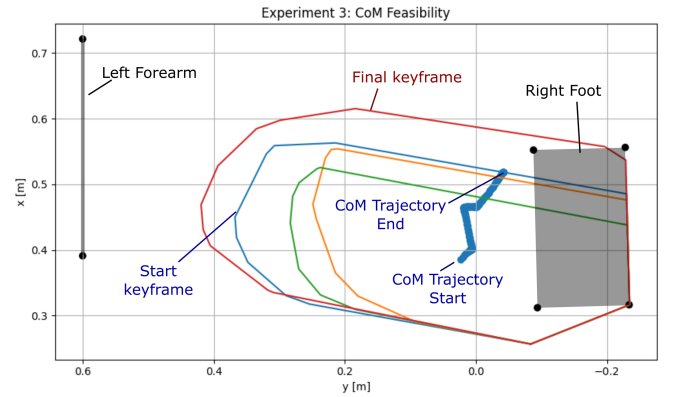


Fig. 6: The trajectory for experiment 3 consists of 4 keyframes as the robot is braced against a wall. This top-down view shows the CoM trajectory along with the set of keyframe CoM constraint regions. The regions with blue, orange, green and red outlines correspond to the feasible CoM regions in keyframes 1-4 respectively.

toe-off. Keyframe feasibility and interpolations can be improved by leveraging modern model-predictive control [32] to perform real-time dynamic feasibility assessment. Time-optimal approaches [2] will be explored as a strategy for faster motion execution.

APPENDIX

Feasible CoM Region. Following the approach from Orsolino et al. [3], the extreme feasible planar CoM position $\mathbf{c}_{xy} \in \mathbb{R}^2$ along a query direction $\mathbf{a} \in \mathbb{R}^2$ is computed as:

$$\begin{aligned} \max_{\mathbf{c}_{xy}, \mathbf{f}} \mathbf{a}^T \mathbf{c}_{xy} \quad \text{s.t.} \quad & \mathbf{A}_f \mathbf{f} + \mathbf{A}_c \mathbf{c}_{xy} = \mathbf{b}_f \\ & \mathbf{C}_f \mathbf{f} \leq \mathbf{d}_f \end{aligned} \quad (8)$$

Where $\mathbf{A}_f, \mathbf{A}_c, \mathbf{b}_f, \mathbf{C}_f, \mathbf{d}_f$ are the constraints in Eq. 4. The equality constraint enforces static equilibrium and the inequality constraint unilateral contact forces, friction constraints, and actuation limits. When solving Eq. 8 for a given direction \mathbf{a}_i , the optimized CoM value \mathbf{c}_{xy}^* lies on the boundary of the feasible CoM region. By querying in a set of directions, an approximation of the feasible CoM region is determined.

Static Force Distribution An optimal static force distribution is computed similarly to Eq. 8 but with \mathbf{c}_{xy} constrained to the keyframe's current position.

$$\min_{\mathbf{f}} \|\mathbf{f}\|_2^2 \text{ s.t. } \mathbf{A}_f \mathbf{f} = \mathbf{b}_f - \mathbf{A}_c \mathbf{c}_{xy} \quad (9)$$

$$\mathbf{C}_f \mathbf{f} \leq \mathbf{d}_f$$

Valkyrie Impedance Gains Tab. V is the set of loaded joint stiffness and damping values used for Experiment 2. A limb is considered loaded when any link contains a contact anchor. Unloaded gains are computed by reducing the loaded gain by a factor of 0.65.

TABLE V: Hardware Loaded Joint Impedance Gains

Joint	Stiffness [N m rad ⁻¹]	Damping [N m s rad ⁻¹]
Sh. Pitch	1600	32
Sh. Roll	1750	50
Sh. Yaw	550	12
El. Pitch	900	30
Hip Yaw	1600	32
Hip Roll	2000	55
Hip Pitch	2000	55
Knee Pitch	2000	60
Ankle Roll	800	10
Ankle Pitch	800	10
Spine Yaw	1750	65
Spine Pitch	1500	45
Spine Roll	1250	55

REFERENCES

- [1] Timothy Bretl and Sanjay Lall. "Testing static equilibrium for legged robots". In: *IEEE Transactions on Robotics* 24.4 (2008), pp. 794–807.
- [2] Quang-Cuong Pham. "A general, fast, and robust implementation of the time-optimal path parameterization algorithm". In: *IEEE Transactions on Robotics* 30.6 (2014), pp. 1533–1540.
- [3] Romeo Orsolino et al. "Feasible region: An actuation-aware extension of the support region". In: *IEEE Transactions on Robotics* 36.4 (2020), pp. 1239–1255.
- [4] Steve Tonneau et al. "An efficient acyclic contact planner for multiped robots". In: *IEEE Transactions on Robotics* 34.3 (2018), pp. 586–601.
- [5] Karim Bouyarmane et al. "Multi-contact motion planning and control". In: *Humanoid Robotics: A Reference* (2018), pp. 1–42.
- [6] Thomas R Groechel et al. "A Tool for Organizing Key Characteristics of Virtual, Augmented, and Mixed Reality for Human-Robot Interaction Systems: Synthesizing VAM-HRI Trends and Takeaways". In: *IEEE Robotics & Automation Magazine* 29.1 (2022), pp. 35–44.
- [7] Emily Sheetz et al. "Comparing Human Input in RViz and Virtual Reality Interfaces for 3D Object Manipulation Tasks". In: *First International Workshop on Horizons of an Extended Robotics Reality at IEEE IROS 2022*.
- [8] Stanislas Brossette, Adrien Escande, and Abderrahmane Kheddar. "Multicontact postures computation on manifolds". In: *IEEE Transactions on Robotics* 34.5 (2018), pp. 1252–1265.
- [9] Quentin Rouxel et al. "Multicontact motion retargeting using whole-body optimization of full kinematics and sequential force equilibrium". In: *IEEE/ASME Transactions on Mechatronics* 27.5 (2022), pp. 4188–4198.
- [10] Naoki Hiraoka et al. "Online generation and control of quasi-static multi-contact motion by PWT Jacobian matrix with contact wrench estimation and joint load reduction". In: *Advanced Robotics* 35.1 (2021), pp. 48–63.
- [11] Bernd Henze et al. "Multi-contact balancing of humanoid robots in confined spaces: Utilizing knee contacts". In: *2017 IEEE/RSJ International Conference on Intelligent Robots and Systems (IROS)*. IEEE. 2017, pp. 697–704.
- [12] Matteo Parigi Polverini et al. "Multi-contact heavy object pushing with a centaur-type humanoid robot: Planning and control for a real demonstrator". In: *IEEE Robotics and Automation Letters* 5.2 (2020), pp. 859–866.
- [13] Kazuya Otani and Karim Bouyarmane. "Adaptive whole-body manipulation in human-to-humanoid multi-contact motion retargeting". In: *2017 IEEE-RAS 17th International Conference on Humanoid Robotics (Humanoids)*. IEEE. 2017, pp. 446–453.
- [14] Kourosh Darvish et al. "Teleoperation of Humanoid Robots: A Survey". In: *arXiv preprint arXiv:2301.04317* (2023).
- [15] Matthew Johnson et al. "Team IHMC's lessons learned from the DARPA Robotics Challenge: Finding data in the rubble". In: *Journal of Field Robotics* 34.2 (2017), pp. 241–261.
- [16] Matt Zucker et al. "A general-purpose system for teleoperation of the DRC-HUBO humanoid robot". In: *Journal of Field Robotics* 32.3 (2015), pp. 336–351.
- [17] Pat Marion et al. "Director: A user interface designed for robot operation with shared autonomy". In: *The DARPA Robotics Challenge Finals: Humanoid Robots To The Rescue* (2018), pp. 237–270.
- [18] Adrien Escande, Abderrahmane Kheddar, and Sylvain Miossec. "Planning contact points for humanoid robots". In: *Robotics and Autonomous Systems* 61.5 (2013), pp. 428–442.
- [19] Joris Vaillant et al. "Multi-contact vertical ladder climbing with an HRP-2 humanoid". In: *Autonomous Robots* 40.3 (2016), pp. 561–580.
- [20] Nancy S Pollard et al. "Adapting human motion for the control of a humanoid robot". In: *Proceedings 2002 IEEE international conference on robotics and automation (Cat. No. 02CH37292)*. Vol. 2. IEEE. 2002, pp. 1390–1397.
- [21] Sungjoon Choi and Joohyung Kim. "Towards a natural motion generator: A pipeline to control a humanoid based on motion data". In: *2019 IEEE/RSJ International Conference on Intelligent Robots and Systems (IROS)*. IEEE. 2019, pp. 4373–4380.
- [22] Alessandro Di Fava et al. "Multi-contact motion retargeting from human to humanoid robot". In: *2016 IEEE-RAS 16th international conference on humanoid robots (humanoids)*. IEEE. 2016, pp. 1081–1086.
- [23] Patrick Beeson and Barrett Ames. "TRAC-IK: An open-source library for improved solving of generic inverse kinematics". In: *2015 IEEE-RAS 15th International Conference on Humanoid Robots (Humanoids)*. IEEE. 2015, pp. 928–935.
- [24] David E Orin and Ambarish Goswami. "Centroidal momentum matrix of a humanoid robot: Structure and properties". In: *2008 IEEE/RSJ International Conference on Intelligent Robots and Systems*. IEEE. 2008, pp. 653–659.
- [25] Mark W Spong, Seth Hutchinson, and Mathukumalli Vidyasagar. *Robot modeling and control*. John Wiley & Sons, 2020.
- [26] Francesco Bullo and Richard M Murray. "Proportional derivative (PD) control on the Euclidean group". In: (1995).
- [27] Roy Featherstone. *Rigid body dynamics algorithms*. Springer, 2014.
- [28] Ken Shoemake. "Animating rotation with quaternion curves". In: *Proceedings of the 12th annual conference on Computer graphics and interactive techniques*. 1985, pp. 245–254.
- [29] Pasquale Chiacchio, Yann Bouffard-Vercelli, and François Pierrot. "Force polytope and force ellipsoid for redundant manipulators". In: *Journal of Robotic Systems* 14.8 (1997), pp. 613–620.
- [30] "Valve Index". [Online]. Available: <https://www.valvesoftware.com/en/index/>. Accessed: 2023-02-15.
- [31] "jMonkeyEngine". [Online]. Available: <https://jmonkeyengine.org/>. Accessed: 2023-02-15.
- [32] Carlos Mastalli et al. "Crocodyl: An efficient and versatile framework for multi-contact optimal control". In: *2020 IEEE International Conference on Robotics and Automation (ICRA)*. IEEE. 2020, pp. 2536–2542.